RESEARCH PAPER

Investigation on Surface Hardness and Microstructure Evolution in AA 7075-T651 Multi-Layered Laminate Fabricated Through Friction Stir Additive Manufacturing

Adeel Hassan[1,*], Mokhtar Awang[1], Srinivasa Rao Pedapati[2], Khurram Altaf[1], Naveed Ahmed[3], Roshan Vijay Marode[1], Syed Waqar Ahmed[1], Imtiaz Ali Soomro[4]

** adeel_21002773@utp.edu.my*

[1] Department of Mechanical Engineering, Universiti Teknologi PETRONAS, Seri Iskandar 32610, Perak Darul Ridzuan, Malaysia

[2] College of Engineering, The University of Texas Permian Basin, 11105 West Highway 191Midland, Texas, 79705, USA

[3] Department of Industrial Engineering, College of Engineering and Architecture, Al-Yamamah University, Riyadh 11512, Saudi Arabia

[4] Department of Metallurgy and Materials Engineering, Mehran University of Engineering and Technology, Jamshoro 76062, Sindh, Pakistan

Received: August 2023 **Revised: December 2023** **Accepted: December 2023**
DOI: 10.22068/ijmse.3361

Abstract: *Friction stir additive manufacturing (FSAM) is a variant of sheet lamination additive manufacturing used to produce large, near-net-shaped 3D parts. Unlike traditional friction stir lap welding, FSAM introduces a new plate to one that is already joined, with the effective area limited to the nugget zone. The present study focuses on exploring the microstructure and microhardness around the nugget zone in a five-plate AA 7075-T651 laminate synthesized at 1000 rpm and 35 mm/min. Microhardness increased vertically in the weldment NZ, reaching 143 HV in the top layer with 2.0 µm fine equiaxed grains. The grains on the advancing and retreating sides were coarser compared to the nugget zone. A W-shaped microhardness profile appeared across layer interfaces. These findings contribute significantly to advancing the FSAM technique, particularly in manufacturing multi-layered, multi-pass laminates.*

Keywords: *Friction stir additive manufacturing (FSAM), AA 7075, Surface hardness, Microstructure evolution, Grain refinement.*

1. INTRODUCTION

AA 7075 is a precipitate-hardened alloy containing zinc, copper, and magnesium as primary alloying elements, making it a popular choice in the automotive and aerospace industries for applications requiring high strength [1, 2]. Due to its superior structural efficiency, this alloy is widely used in the aerospace industry for wing spars, cabin and cockpit components, spacecraft chassis, and planetary rover wheels [3, 4]. Conventional techniques such as casting, welding, and forging are commonly used to manufacture these extremely large, irregularly shaped components [5]. However, a very sluggish cooling rate in the casting process increases the degree of segregation, and heterogeneous microstructure results in mechanical properties inferior to base metal [6].

Similarly, the welding process involves melting, which causes excessive splashing and vaporization of zinc, resulting in severe cracking and solidification defects as well as high-textured columnar grains [7, 8]. Due to this, the aluminum 7000 series is deemed a non-fusion weldable series. The current metal-based additive manufacturing (MAM) techniques employ a very high energy beam to melt the feed material, which is similar to micro-welding [9, 10]. Therefore, components of this alloy cannot be manufactured additively without altering the composition of the base metal [5, 11]. Moreover, current MAM techniques have a very low building rate and are unsuitable for fabricating medium-to-large components [12]. The alternative route is machining out the parts from the billet and assembling them with nuts and bolts, which is not flight-qualified for spacecraft components and results in substantial material wastage.

Consequently, to surmount the aforementioned limitations, an alternative manufacturing method is required to produce large, irregularly shaped parts with enhanced mechanical properties and a high build rate. Solid-state additive

[DOI: 10.22068/ijmse.3361]

manufacturing would be a suitable approach for addressing such challenges. As no fusion or melting is involved in solid-state manufacturing, the materials are bonded together by severe plastic deformation. Among the well-known solid-state additive manufacturing processes, friction stir additive manufacturing (FSAM) is a relatively new technique that Mr. White proposed in 2002 [13] and that lies under sheet lamination additive manufacturing [10]. Large, near-net-shaped parts with a low level of complexity could be manufactured with a high production rate and efficient mechanical and microstructural properties. However, FSAM is in the initial stage and still faces challenges. Achieving highly complex parts is difficult, and the manufactured components may exhibit non-homogeneous mechanical properties. Additionally, post-machining is required to obtain the final part, and special fixtures are necessary for clamping.

Below the melting point, the feed material in the plate form is joined using a non-consumable rotating tool. The working principle of FSAM is similar to the conventional friction stir lap welding (FSLW), but the process changed drastically after adding the second layer. After removing the flash (produced during the stirring process), it is necessary to add an additional layer by repeating the stirring process until the desired height is attained. The near-net-shaped laminate was then machined to produce the final component. Fig. 1 depicts the steps involved in the FSAM process. Overall, less post-machining is required in FSAM compared to billet-to-part fabrication through machining.

FSAM technique proposed by Mr. White [13] was subsequently adopted for the first time by Boeing and Airbus [15, 16], and they pronounced it to be an energy-efficient process with high mechanical properties and build rate. After that, Palanivel et al. [17, 18] developed AA 5083 and magnesium alloy WE43 multi-layered laminates and reported high microhardness compared to the base metal in the nugget zone along the building direction. In recent years, FSAM has rapidly risen to prominence among researchers. Numerous researchers have investigated both identical materials [18, 19, 20, 21, 22] and multi-material laminates [23, 24, 25, 26], in the context of FSAM.

However, laminates of Al-Zn-Mg-Cu alloy have also been studied in both dry [27, 28, 29, 30] and underwater FSAM [31, 32, 33]. These studies focused on single-track multi-layered laminates and mechanical hardness and microstructure were analyzed in the building direction. Similarly, M. Liu [34] and S. Wlodarski [35] accomplished multi-track, multi-layered laminates of pure copper and magnesium alloy (AZ31), respectively through FSAM by applying overlapping the nugget zone technique.

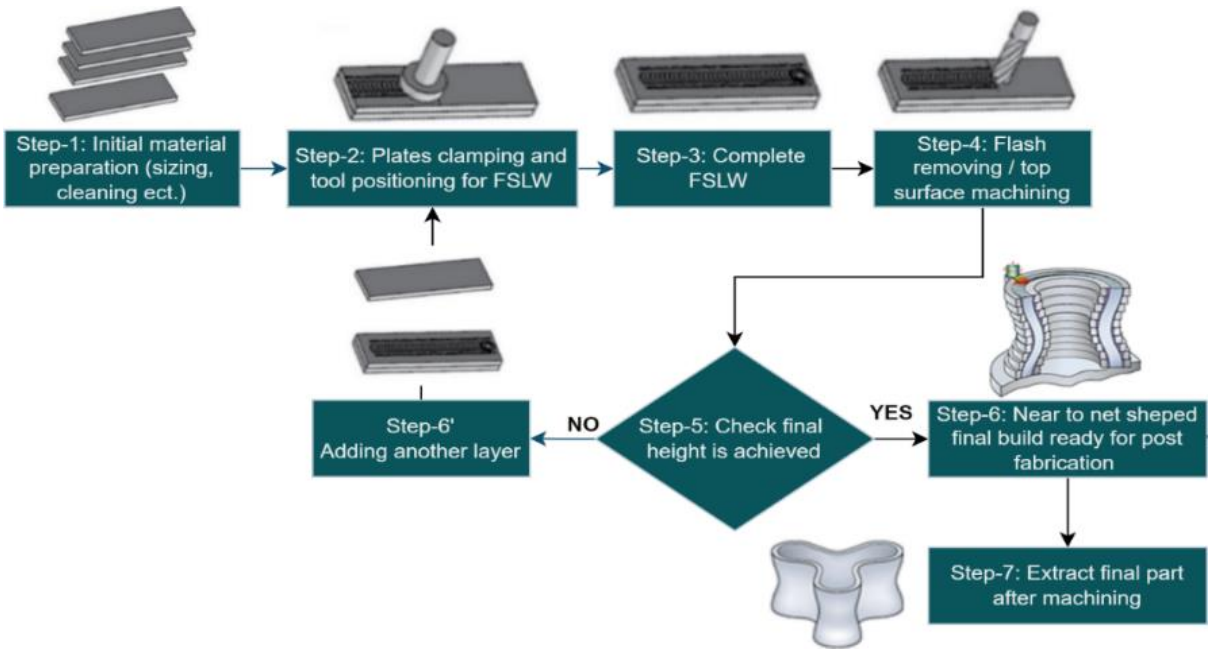

Fig. 1. FSAM process schematic illustration [14]

[DOI: 10.22068/ijmse.3361]

The majority of the FSAM studies focused on microhardness and microstructure exploration of the nugget zone center along the building direction. Microhardness and microstructure distribution around the nugget zone-NZ (Advancing side-AS, Retreating side-RS) of two-plate laminates in lap and butt configurations have been extensively studied in the literature [36, 37, 38, 39]. Before fabricating large area (multi-track) multi-layered laminates, it is necessary to investigate the microstructure and surface hardness of NZ, AS, and RS of already bonded layers because the previously boded layers have been altered mechanically and microstructurally in comparison to the new layer. In the present study, a five-layered laminate of aerospace alloy AA 7075-T651 was manufactured with a threaded H13 tool. Therefore, an attempt was made to explore the microstructure evolution and microhardness distribution in the nugget zone, as well as in the AS and RS of each layer's interfaces. The findings of the present study aid in creating the multi-layered laminate of AA 7075-T651, having a larger area.

2. EXPERIMENTAL PROCEDURES

The commercially available 6 mm thick AA 7075 plates in T651 condition were used to make a multi-layered laminate of 42 mm height. The chemical composition of the base material is shown in TABLE 1. Before the FSAM experiments, the base palates were cleaned with acetone to remove surface impurities such as oil, grease, dirt, etc. Acetone was used for this purpose because it is a highly effective solvent to dissolve these impurities and evaporates quickly after cleaning. A non-consumable FSAM tool having a taper threaded pin longer than the thickness of the base plate, made of H13 tool steel, was fabricated using a conventional medium-duty lathe machine. Moreover, the tool was heat-treated to achieve a higher hardness of 45-50 HRC so that it may not break during the processing. The heat treatment cycle [40, 29] (~9 hours) comprises preheating at 900°C, austenitizing at 1050°C, oil quenching, and then tempering at 600°C. The complete heat treatment cycle applied on the FSAM tool is shown in Fig. 2.

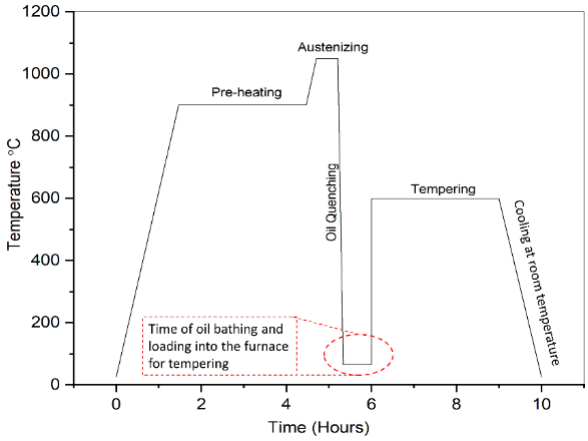

Fig. 2. Heat treatment cycle applied on FSAM tool

To obtain multi-layered FSAM laminate, a dedicated numeric control friction stir welding machine (FSW-TS-F16, China-made) was used at a rotational speed of 1000 rpm. A heat-treated FSAM tool (non-consumable) having a taper threaded pin longer than base plate thickness was used to accomplish the laminate. The illustration of the final five-layered laminate and actual FSAM tool is shown in Fig. 3. Initially, the tool plunged continuously for 10 seconds (dwelling time) in firmly clamped base plates to attain a specific temperature. To achieve the accurate plunge depth of 0.3 mm, the value was set in the numeric control panel of the machine, and the tool was then moved at a constant transverse velocity of 35 mm/min to complete an 80 mm long weld track. These parameters were tuned to achieve defect-free laminate after lots of trial experiments. The complete set of operating parameters opted for the present work is displayed in TABLE 2. To investigate the microstructure and micro-hardness of the bonded layers, rectangular samples encompassing various areas, such as the nugget zone, heat-affected zone, and thermo-mechanically affected area, were cut using a wire-cut electric discharge machine-EDM.

Table 1. Chemical composition (%) of feed material

AA 7075-T651– Chemical composition (wt%)				
Si	Fe	Cu	Mn	Mg
0.087	0.31	1.40	0.16	2.52
Cr	Zn	Ti	Al	-
0.211	5.450	0.037	rest	-

[DOI: 10.22068/ijmse.3361]

Table 2. FSAM operating parameters

FSAM tool parameters	Tool pin profile	Taper threaded
	Pin length	8 mm
	Pin diameter d_1/d_2	8 mm/6 mm
	Shoulder type	flat
	Shoulder diameter	24 mm
Machine parameters	Plunge depth	0.3 mm
	Rotational speed	1000 rpm
	Transverse speed	35 mm
	Tilt angle	2.5°
Feed material parameters	Plate thickness	6 mm
	Dimensions (W×L)	100 × 150 mm
	No. of plates joined	5 plates

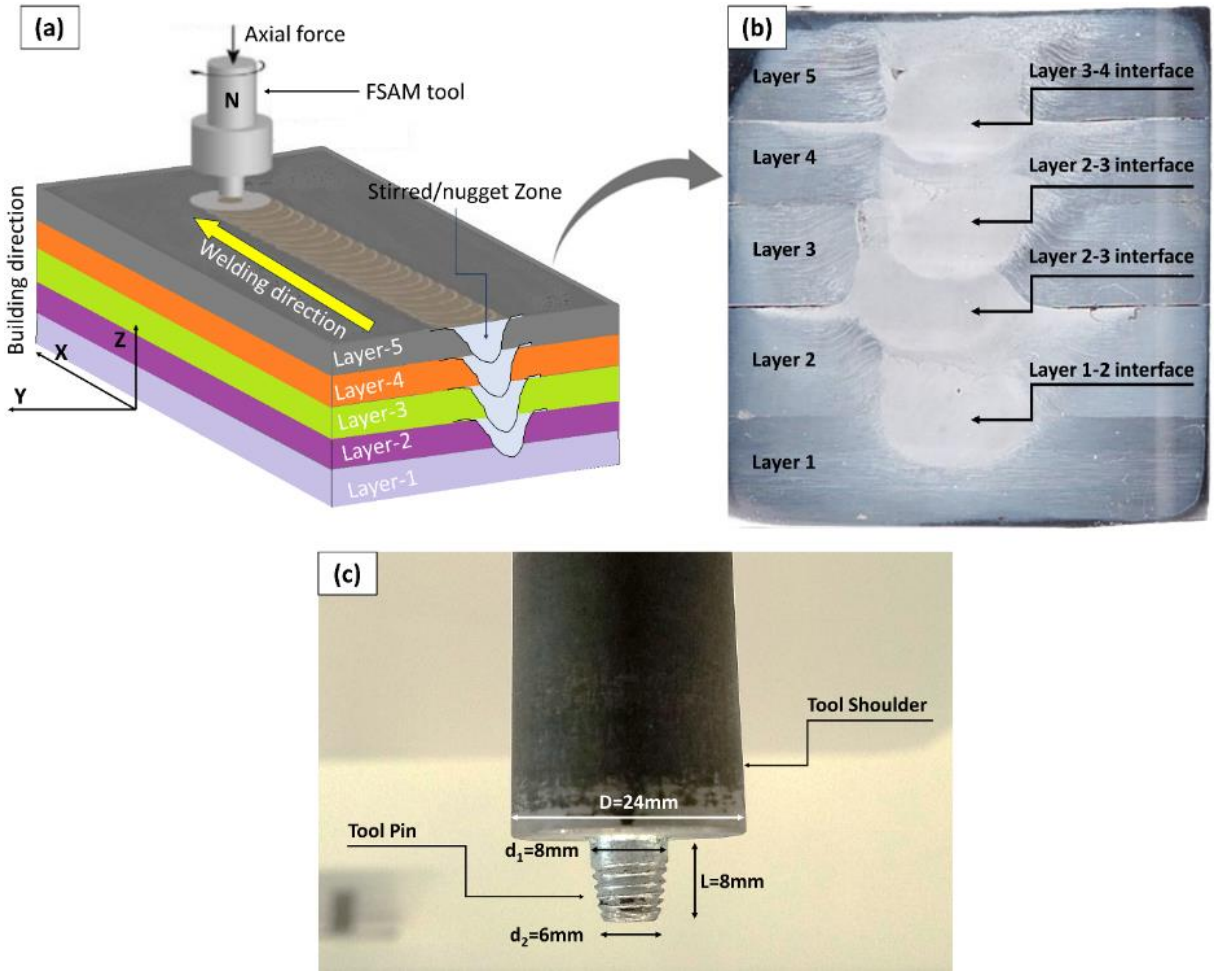

Fig. 3. (a) Illustration of final five-layered laminate (b) Cross-sectioned view of actual manufactured laminate (c) FSAM tool

Following standard metallographic procedures [41], a mirror-polished surface was achieved. From the center of the nugget zone, the surface hardness and microstructure of each layer interface were analyzed in both the building and horizontal directions. Vickers's hardness tester (LM 247AT-Leco, HQ: LV Ave, St. Joseph, MI, USA) was used at room temperature with a 500-gram load to measure hardness, and a Leica metallographic optical microscope (Leica DM LM, Germany) was used to characterize the microstructure. Before microstructure characterization, the mirror-polished samples were chemically etched for 15-20 seconds using

[DOI: 10.22068/ijmse.3361]

Keller's reagent (HF- 3 ml, HCL- 2 ml, HNO_3- 5 ml, H_2O- 195 ml) to reveal the different microstructure zones. The microstructure images were captured using an optical microscope with a 50X magnification lens. In addition, scaled images were imported to the software ImageJ (V1.53e, NIH, USA) to analyze the grain size distribution, and a minimum of 100 grains were measured for each layer interface.

3. RESULTS AND DISCUSSION

3.1. Microstructure Evolution

The microstructure of nugget zone-NZ, advancing side-AS, and retreating side-RS were investigated in terms of grain refinement. Following the line intercept method, at least 100 particles per layer interface were measured. The micrographs of actual grains obtained with an optical microscope (OM) at 50X magnification are shown in Fig. 4. The results were then plotted in Fig. 5 as a histogram to estimate the average grain size. In Fig. 5, the average grain size in the AS and RS of the weldment is presented in black color (a_1-a_4) and red color (c_1-c_4) respectively. However, the grain size attained in the NZ of each interface is displayed in blue color (b_1-b_4).

At interface 1-2, precipitates in the advancing and retracting sides are coarser compared to the nugget zone, as shown in Fig. 4. The precipitates are identical to the base material (BM) because the first interface has not undergone plastic deformation as the layers are bonded in lap configuration. Whereas precipitates at the interfaces of the 3rd, 4th, and 5th layers were finer because these regions came in contact with the tool shoulder once.

Overall, grains in the AS are more refined than RS at the same interface, but their size decreases gradually as the number of layers increases. The precipitates in the nugget zone are much finer in comparison to AS and RS because the stir zone agitated twice. The top of the already stacked lap was first time stirred with the action of the tool shoulder and the second time stirred with the tool pin during the addition of the new layer. A similar phenomenon was also well explained graphically by Mr. Y. Li [33] in his study FSAM in the water bath.

As the build height increases, the grain size is going to decrease. Macroscale softening is the primary reason behind this occurrence. Similar trends were also reported by other researchers [28, 32] in their studies. The macroscale effect could be eliminated by opting the FSAM in the water [31]. The overall summary of grain refinement is depicted in the 3D bar graph Fig. 6. The minimum of 2.0 μm diameter grains was achieved in the nugget zone of layers 4 and 5 interface whereas the maximum 8.53 μm was found in the AS of layers 1 and 2 interface.

3.2. Surface Hardness

Hardness is a very effective property of the material, which presents the local resistance of that material, which further helps to estimate the strength of the material. A rectangular-shaped sample was taken from the cross-section to evaluate the surface hardness distribution. As illustrated in Fig. 7.a, the cross-sectioned sample includes various zones such as the pin-driven zone-PDZ, the shoulder-driven zone-SDZ, the thermo-mechanically affected zone-TMAZ, and the heat-affected zone-HAZ. In PDZ, the material is just stirred by the action of the tool pin, whereas in SDZ, the material is plasticized by the contact of the tool shoulder. TMAZ is the transition zone between the PDZ (also known as the nugget or stir zone) and the HAZ. Heat-affected zone-HAZ, on the other hand, is the area influenced by the frictional heat created by the FSAM tool but not subjected to significant plastic deformation. Overall, HAZ is larger than TMAZ, but TMAZ was subjected to greater temperatures. Micro-hardness was thus assessed in two directions (horizontal and vertical), covering all zones.

Firstly, the microhardness of the parent material was measured, which was 122 HV, shown in Fig. 8 in blue. After that, the hardness of each layer interface was measured in the horizontal direction with an interval of 0.5 mm, as per the schematic below in Fig. 7b. The microhardness (horizontal direction) obtained in the present work is present in the graphical form below in Fig. 8. Overall, W-shaped hardness profile attained which is very common for heat-treatable aluminum alloys [25, 36, 42]. This is due to the combined effect of dissolution of precipitates and rapid cooling of bonded material behind the tool. Micro-hardness values of the NZ are approximately stable compared to the AS and RS (TMAZ+HAZ). NZ hardness of layer 1, 2 interface and layer 2, 3 interface was lower than the base metal whereas, layer 3, 4 interface and

[DOI: 10.22068/ijmse.3361]

layer 4, 5 interface have improved hardness compared to the BM.

Generally, the average hardness of each layer interface in the AS was slightly higher compared to the RS. This is due to the high temperature in the AS resulting from the plasticized material flow from the RS (colder material) with the tool pin. This high temperature could cause the breaking of coarser grains and strengthening precipitate dissolution [43]. As already explained, in FSAM, the effective area is the only nugget zone, so a maximum hardness of 143 HV at NZ of layer 4, 5 interface was recorded. The average hardness of the NZ at layer interfaces 1-2, 2-3, 3-4, and 4-5 was 108.24 HV, 108.54 HV, 126.26 HV, and 131.58 HV, respectively. Nevertheless, the difference in hardness between the topmost layer interface 4-5 and interfaces 1-2, 2-3, and 3-4 was 21.56%, 21.22%, and 4.21%, respectively.

Surface hardness in the build direction (vertically) was also measured as per Fig. 9a to explore the effect of multi-layer addition. Microhardness was recorded on the center line of NZ after a 0.5 mm distance. Microhardness increases steadily from the bottom to the top, as shown in Fig. 9b. The results were agreed with the findings of other researchers [25, 28, 32]. At the bottom, the hardness was lower, whereas the maximum hardness was found to be 142 HV at the topmost layer. The primary root cause of this happening is the thermal cycling effect.

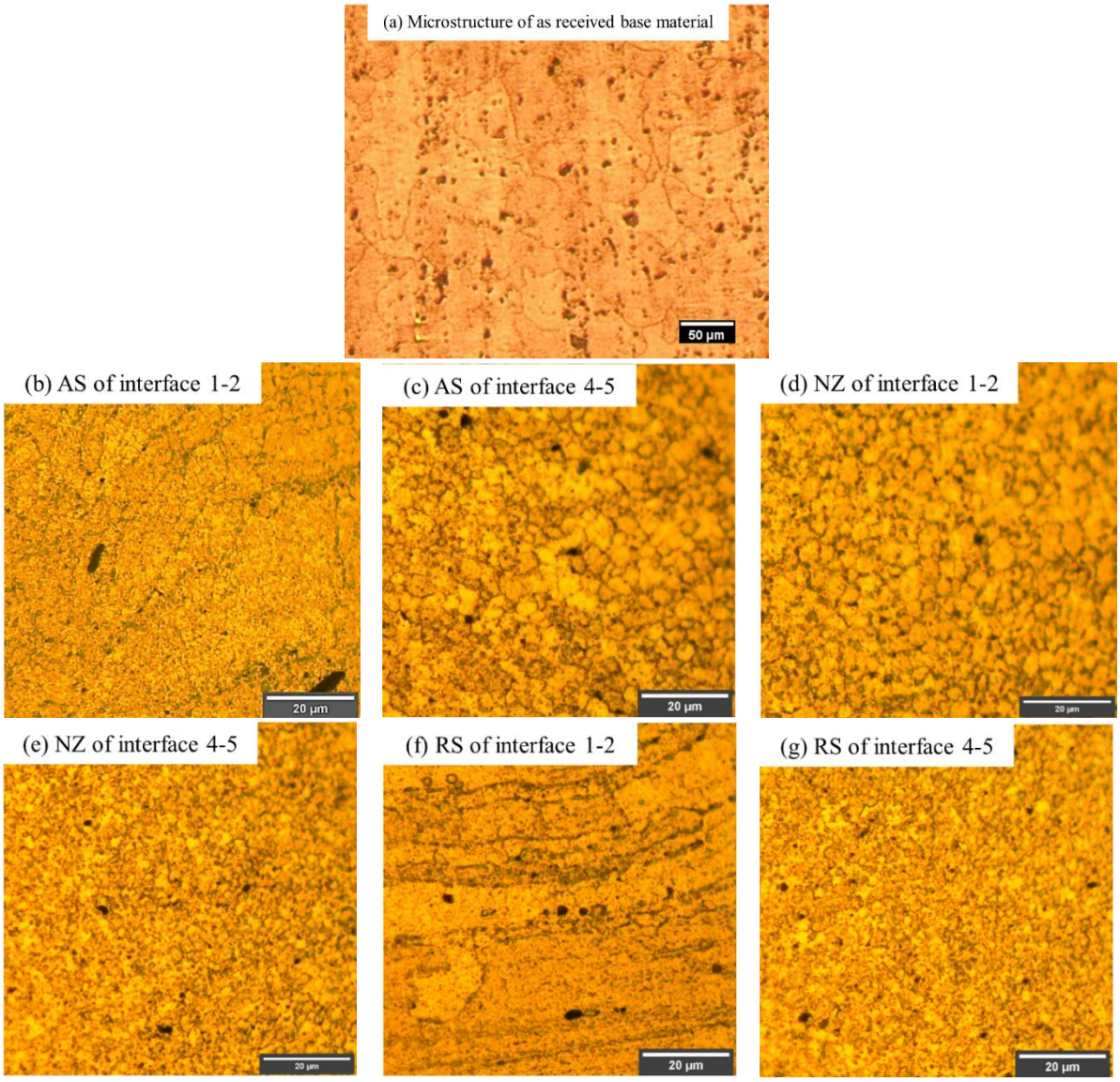

Fig. 4. OM micrographs of BM, AS, NZ, RS of weldment interface 1-2 & 4-5 at 50X magnification

[DOI: 10.22068/ijmse.3361]

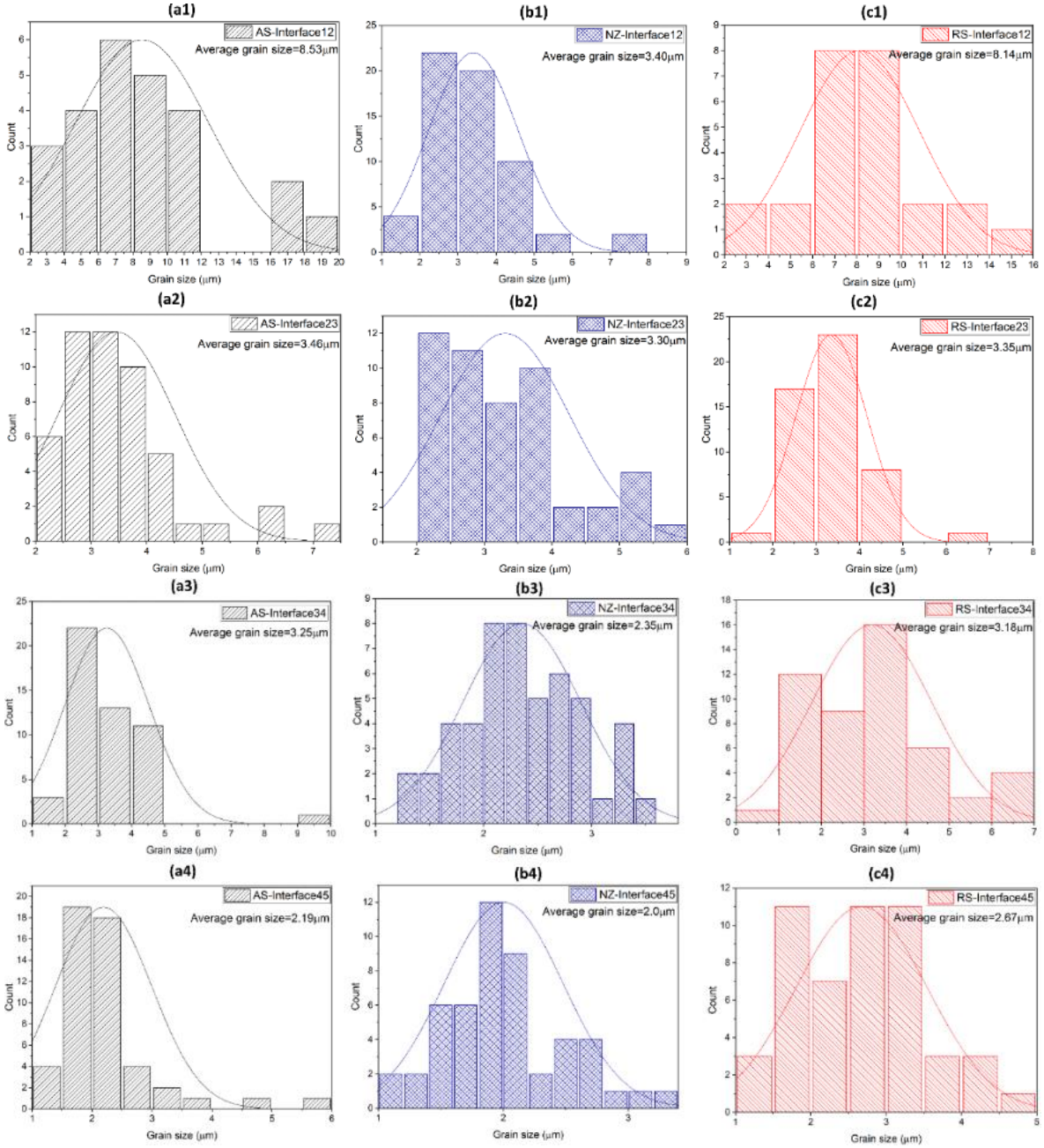

Fig. 5. Grains distribution in the weldment: (a_1-a_4) average grain size of each interface in AS; (b_1-b_4) average grain size of each interface in NZ; (c_1-c_4) average grain size of each interface in RS

In addition to each new layer, the already bonded layers were exposed to frictional heat every time, whereas the last plate only experienced heat once. As a result, the grains from top to bottom get coarser.

Overall, the average surface hardness along the centerline of NZ was 123.6 HV, which is nearly equal to the BM hardness (122 HV). If we correlate it with the grain refinement, the average grains in the stir zone were about 4 times reduced. Thus, it might be concluded that the microhardness of heat-treatable aluminum alloy depends not only on grain refinement. It might depend on other factors like dissolution, distribution, and dislocation density of strengthening precipitates. So, controlling the distribution and dissolution of the strengthening precipitates in FSAM is quite challenging due to the variable and high thermal exposure. This could be achieved through some statistical techniques such as Taguchi or Response Surface Methodology.

[DOI: 10.22068/ijmse.3361]

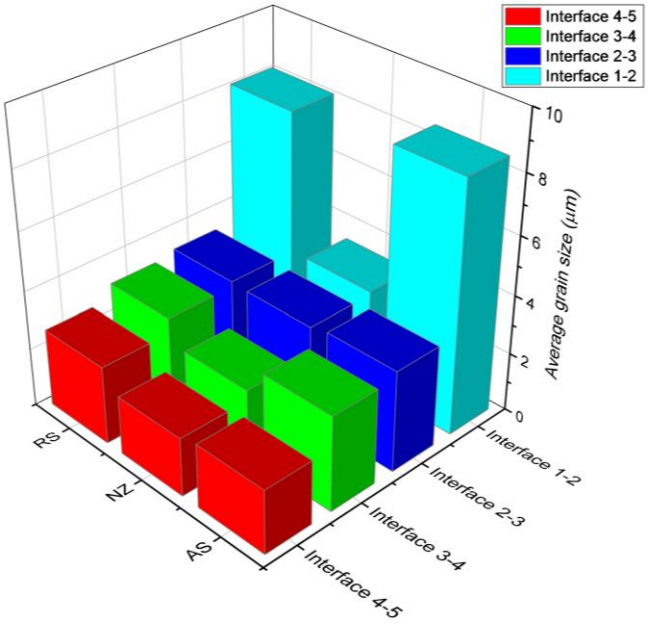

Fig. 6. Comparable breakdown of grain refinement

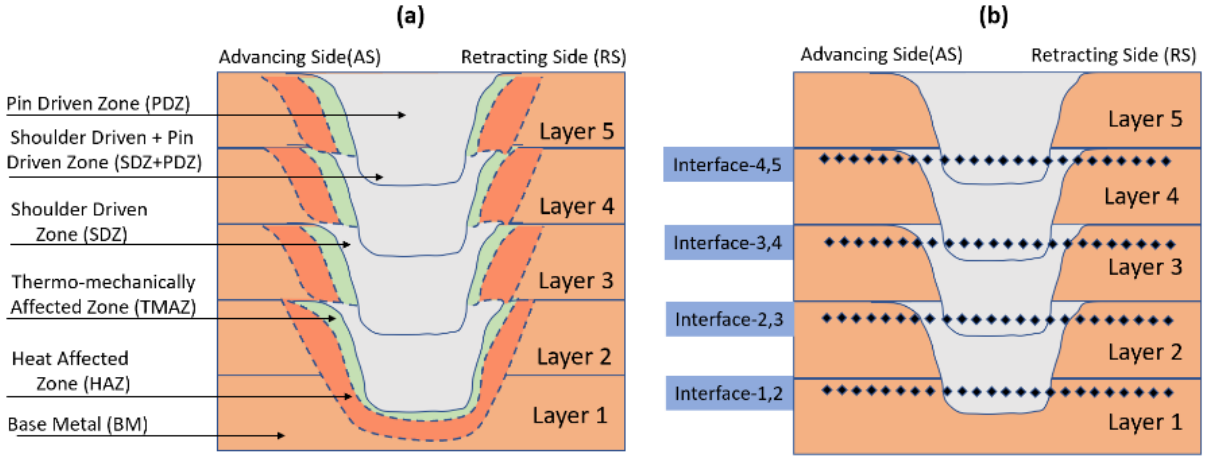

Fig. 7. (a) Graphical illustration of different zones of laminate; (b) Horizontal hardness measurement plan

4. CONCLUSIONS

The five-layered defect-free laminate of AA 7075-T651 was produced using the FSAM technique. The microstructure evolution and microhardness distribution around the nodule zone were investigated in the horizontal and vertical directions. The following are the primary conclusions of the present study.

- Particles in the nugget zone are substantially finer compared to the advancing and retreating side. Whereas grains on both advancing and retreating sides are almost the same.

Grains become coarser from the layer 5, 6 interface to the layer 1, 2 interface. A minimum of 2.0 μm grain size was achieved in the nugget zone of layers 4 and 5 interface whereas the maximum 8.53 μm was found in the AS of layers 1 and 2 interface.

- Overall, the microhardness of AS was slightly lower compared to RS in the horizontal direction around the NZ of each layer interface. However, the average NZ hardness of each layer interface was higher than that of AS and RS due to the refined grain size. Maximum hardness 131.58 HV of layer 4, 5 interface was observed.
- In the vertical direction, the micro-hardness of weldment NZ along the center line was discovered to be directly proportional to the building height. The topmost layer's NZ had the highest hardness of 143 HV.

[DOI: 10.22068/ijmse.3361]

- The microhardness of heat-treatable alloy (AA 7075-T651) is not dependent on the grain size only; it might depend on the other microstructural parameters such as precipitate distribution, dissolution, and dislocation density. Further study is underway to explore these parameters.

ACKNOWLEDGEMENT

The authors wish to acknowledge Mr. Hafiz bin Safian, senior technologist from the Engineering Prototyping & Innovation Center at Universiti Teknologi PETRONAS, for providing FSAM facilities and valuable assistance.

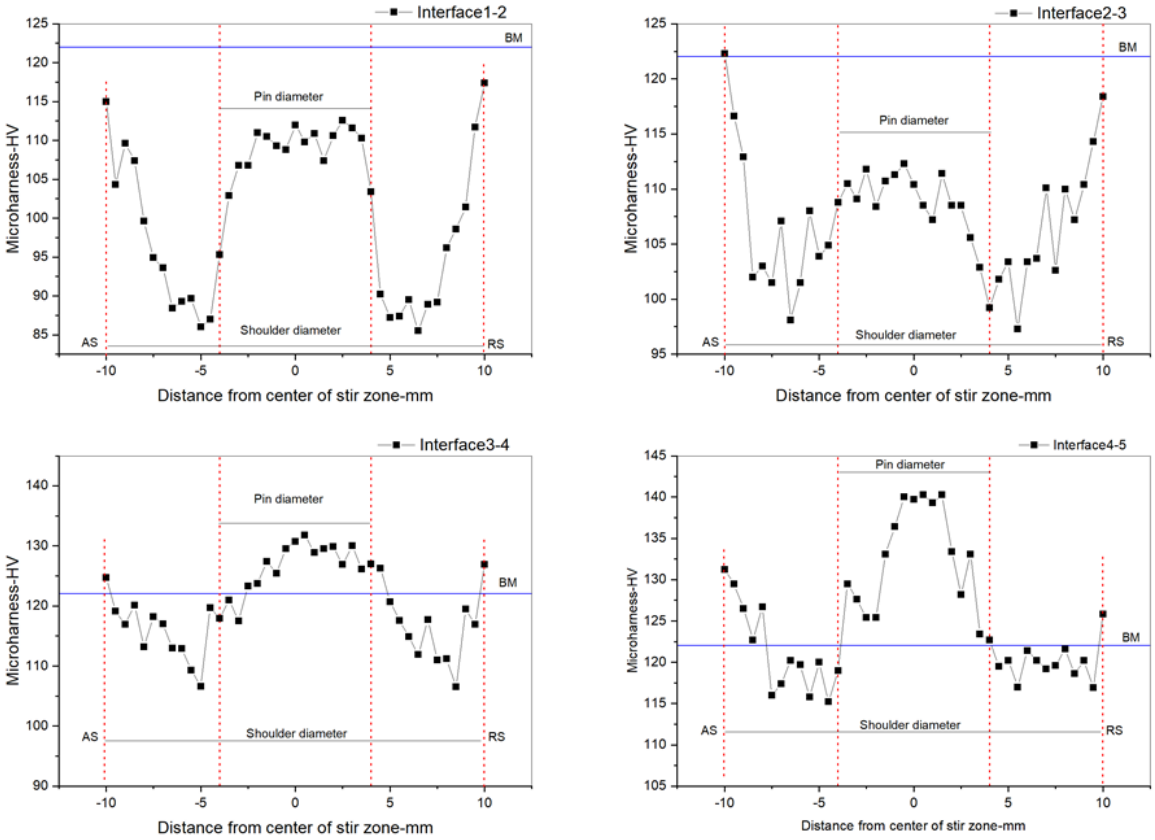

Fig. 8. Microhardness distribution across each layer interface

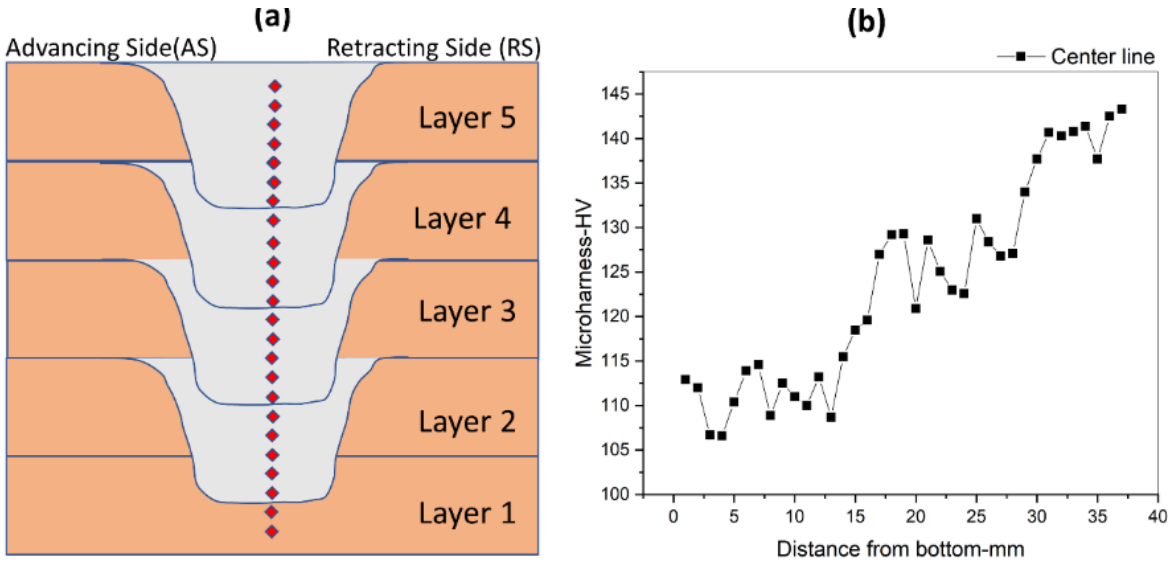

Fig. 9. (a) Schematic of NZ hardness measurement along building direction; (b) experimental NZ microhardness in the build direction

[DOI: 10.22068/ijmse.3361]

REFERENCES

[1]. Davis JR., "Aluminum and aluminum alloys". ASM international; 1993.

[2]. Lotfi AH, Nourouzi S., "Predictions of the optimized friction stir welding process parameters for joining AA7075-T6 aluminum alloy using preheating system". Int J Adv Manuf Technol., 2014, 73:1717–37.

[3]. Jawalkar CS, Kant S., "A review on use of aluminium alloys in aircraft components". i-Manager's J Mater Sci., 2015, 3(3):33.

[4]. Dehghani K, Ghorbani R, Soltanipoor AR., "Microstructural evolution and mechanical properties during the friction stir welding of 7075-O aluminum alloy". Int J Adv Manuf Technol., 2015, 77:1671–9.

[5]. Oropeza D, Hofmann DC, Williams K, Firdosy S, Bordeenithikasem P, Sokoluk M, et al., "Welding and additive manufacturing with nanoparticle-enhanced aluminum 7075 wire". J Alloys Compd., 2020, 834:154987.

[6]. Babajanzade Roshan S, Behboodi Jooibari M, Teimouri R, Asgharzadeh-Ahmadi G, Falahati-Naghibi M, Sohrabpoor H., "Optimization of friction stir welding process of AA7075 aluminum alloy to achieve desirable mechanical properties using ANFIS models and simulated annealing algorithm". Int J Adv Manuf Technol., 2013, 69:1803–18.

[7]. Palanivel S, Mishra RS., "Building without melting: a short review of friction-based additive manufacturing techniques". Int J Addit Subtractive Mater Manuf., 2017, 1(1):82–103.

[8]. Li L, Li R, Yuan T, Chen C, Zhang Z, Li X., "Microstructures and tensile properties of a selective laser melted Al–Zn–Mg–Cu (Al7075) alloy by Si and Zr microalloying". Mater Sci Eng A., 2020, 787(April):139492.

[9]. Palanivel S, Nelaturu P, Glass B, Mishra RS., "Friction stir additive manufacturing for high structural performance through microstructural control in an Mg based WE43 alloy". Mater Des., 2015, 65:934–52.

[10]. Gao H, Li H., "Friction additive manufacturing technology: A state of the art survey". Adv Mech Eng., 2021, 13(7):1–29.

[11]. Zhang H, Zhu H, Qi T, Hu Z, Zeng X., "Selective laser melting of high strength Al-Cu-Mg alloys: Processing, microstructure and mechanical properties". Mater Sci Eng A., 2016, 656:47–54.

[12]. Zhang C, Li Y, Gao M, Zeng X., "Wire arc additive manufacturing of Al-6Mg alloy using variable polarity cold metal transfer arc as power source". Mater Sci Eng A., 2018, 711:415–23.

[13]. White D., "Object consolidation employing friction joining". United States Patent: Google Patents; US 6,457,629 B1 Oct. 1, 2002, 2002.

[14]. Hassan A, Pedapati SR, Awang M, Soomro IA., "A Comprehensive Review of Friction Stir Additive Manufacturing (FSAM) of Non-Ferrous Alloys". Vol. 16, Materials. 2023.

[15]. Lequeu P, Muzzolini R, Ehrstrom JC, Bron F, Maziarz R., "High-Performance friction stir welded structures using advanced alloys". In: Aeromat Conference Seattle WA; 2006.

[16]. Baumann JA., "Production of Energy Efficient Preform Structures (PEEPS)". [Internet] The Boeing Company; 2012.

[17]. Palanivel S, Nelaturu P, Glass B, Mishra RS., "Friction stir additive manufacturing for high structural performance through microstructural control in an Mg based WE43 alloy". Mater Des., 2015, 65:934–52.

[18]. Srivastava M, Rathee S., "Microstructural and microhardness study on fabrication of Al 5059/SiC composite component via a novel route of friction stir additive manufacturing". Mater Today Proc., 2020, 39:1775–80.

[19]. Zhao Z, Yang X, Li S, Li D., "Interfacial bonding features of friction stir additive manufactured build for 2195-T8 aluminum-lithium alloy". J Manuf Process., 2019, 38(August 2018):396–410.

[20]. Zhang Z, Tan ZJ, Li JY, Zu YF, Sha JJ., "Integrated Modeling of Process–Microstructure–Property Relations in Friction Stir Additive Manufacturing". Acta Metall Sin Lett., 2020, 33(1):75–87.

[21]. Zhang Z, Tan ZJ, Li JY, Zu YF, Liu WW,

[DOI: 10.22068/ijmse.3361]

Sha JJ., "Experimental and numerical studies of re-stirring and re-heating effects on mechanical properties in friction stir additive manufacturing". Int J Adv Manuf Technol., 2019, 104(1–4):767–84.

[22]. Lu IK, Reynolds AP., "Innovative friction stir additive manufacturing of cast 2050 Al–Cu–Li aluminum alloy". Prog Addit Manuf., 2021, 6(3):471–7.

[23]. Kumar S, Srivastava AK., "Mechanical Properties of Al-Cu-Mg Taylor- made functionally graded layers by Friction Stir Additive Manufacturing". Int J Adv Res Innov ideas Educ IJARIIE., 2021, 7(6):1652–9.

[24]. Derazkola HA, Khodabakhshi F, Simchi A., "Evaluation of a polymer-steel laminated sheet composite structure produced by friction stir additive manufacturing (FSAM) technology". Polym Test., 2020, 90(June):106690.

[25]. Kumar Jha K, Kesharwani R, Imam M., "Microstructural and micro-hardness study on the fabricated Al 5083-O/6061-T6/7075-T6 gradient composite component via a novel route of friction stir additive manufacturing". Mater Today Proc., 2022, 56:819–25.

[26]. Derazkola HA, Mohammadi Abokheili R, Kordani N, Garcia E, Murillo-Marrodán A., "Evaluation of nanocomposite structure printed by solid-state additive manufacturing". CIRP J Manuf Sci Technol., 2022, 37:174–84.

[27]. He C, Li Y, Zhang Z, Wei J, Zhao X., "Investigation on microstructural evolution and property variation along building direction in friction stir additive manufactured Al–Zn–Mg alloy". Mater Sci Eng A., 2020, 777(November 2019):139035.

[28]. Yuqing M, Liming K, Chunping H, Fencheng L, Qiang L., "Formation characteristic, microstructure, and mechanical performances of aluminum-based components by friction stir additive manufacturing". Int J Adv Manuf Technol., 2016, 83(9):1637–47.

[29]. Hassan A, Awang M, Pedapati SR, Altaf K, Marode RV, Ahmed SW., "Experimental investigation on tool pin profile for defect-free multi-layered laminates using friction stir additive manufacturing". Results Eng., 2023, 20(July):101516.

[30]. Sigl ME, Danninger P, Bernauer C, Hartl R, Zaeh MF., "Efficient Build-Up of High-Strength Aluminum Structures Using Friction Stir Additive Manufacturing". Key Eng Mater., 2022, 926(1):176–86.

[31]. Li Y, He C, Wei J, Zhang Z, Qin G, Zhao X., "Correlation of local microstructures and mechanical properties of Al–Zn–Mg–Cu alloy build fabricated via underwater friction stir additive manufacturing". Mater Sci Eng A., 2021, 805(September 2020):140590.

[32]. He C, Li Y, Wei J, Zhang Z, Tian N, Qin G, et al., "Enhancing the mechanical performance of Al–Zn–Mg alloy builds fabricated via underwater friction stir additive manufacturing and post-processing aging". J Mater Sci Technol., 2022, 108(October):26–36.

[33]. Li Y, He C, Wei J, Zhang Z, Tian N, Qin G, et al., "Restirring and Reheating Effects on Microstructural Evolution of Al–Zn–Mg–Cu Alloy during Underwater Friction Stir Additive Manufacturing". Materials (Basel)., 2022, 15(11):3804.

[34]. Liu M, Wang BB, An XH, Xue P, Liu FC, Wu LH, et al., "Friction stir additive manufacturing enabling scale-up of ultrafine-grained pure copper with superior mechanical properties". Mater Sci Eng A., 2022, 857(May):144088.

[35]. Wlodarski S, Avery DZ, White BC, Mason CJT, Cleek C, Williams MB, et al., "Evaluation of Grain Refinement and Mechanical Properties of Additive Friction Stir Layer Welding of AZ31 Magnesium Alloy". J Mater Eng Perform., 2021, 30(2):964–72.

[36]. Kalemba I, Kopyscianski M, Hamilton C, Dymek S., "Natural aging behavior of friction stir welded Al-Zn-Mg-Cu aluminum alloys". Arch Metall Mater., 2015, 60(2A):875–9.

[37]. Kosturek R, Lewczuk R, Torzewski J, Wachowski M, Słabik P., "Research on the post-weld explosive hardening of AA7075-T651 friction stir welded butt joints". Bull POLISH Acad Sci Tech Sci., 2023, :1–7.

[38]. Medhi T, Das A, Pankaj P, Kapil S, Biswas P., "Multi-Pass Friction Stir Lap Welding of AA 6061-T6: Implication of Tool Pin

[DOI: 10.22068/ijmse.3361]

Overlapping on Microstructure and Mechanical Properties of Joints". Soldag e Insp., 2022, 27.
[39]. Kumar G, Kumar R, Kumar R., "Optimization of process parameters of friction stir welded AA5082-AA7075 butt joints using resonance fatigue properties". Bull Polish Acad Sci Tech Sci., 2020, 68(1):99–108.
[40]. Guanghua Y, Xinmin H, Yanqing W, Xingguo Q, Ming Y, Zuoming C, et al., "Effects of heat treatment on mechanical properties of H13 steel". Met Sci Heat Treat., 2010, 52(7–8):393–5.
[41]. ASTM., "E3-11 Standard Guide for Preparation of Metallographic Specimens 1". ASTM Copyright., 2011, i(Reapproved):1–12.
[42]. Kundurti SC, Sharma A., "Evaluation of Microstructural, Mechanical and Corrosion Behaviours of Laminated AA6061/AA7075 Metal Matrix Composites Build by Friction Stir Additive Manufacturing for Structural Applications". Mater Res., 2023, 26.
[43]. Lotfi AH, Nourouzi S., "Predictions of the optimized friction stir welding process parameters for joining AA7075-T6 aluminum alloy using preheating system". Int J Adv Manuf Technol., 2014, 73(9–12):1717–37.

[DOI: 10.22068/ijmse.3361]